Numerical Simulation of the Flow Around Wind Turbines using the Immersed Boundary Method

João E. F. Martini[1], Rafael R. S. Melo[2], Aristeu da Silveira Neto[1]

[1]*Fluid Mechanics Laboratory, Federal University of Uberlândia*
2121 Av. João Naves de Ávila, zip code 38408-100, Uberlândia, Minas Gerais, Brazil
joaoemanuel1996.jem@gmail.com, aristeus@ufu.br
[2]*Department of Thermal Science and Fluids, Federal University of São João del-Rei*
170 Frei Orlando Square, zip code 36307-352, São João del-Rei, Minas Gerais, Brazil
rafaelmelo@ufsj.edu.br

Abstract. The aerodynamics study in wind turbines by computational fluid dynamics (CFD) techniques is fundamental since these tools help improve the performance of wind turbines and the choice of design of the rotor blades more efficient. Thus, we perform a computational simulation to (i) obtain the lift and drag coefficients of the s809 airfoil (ii) obtain the torque and power of the NREL PHASE VI wind turbine. The wind turbine simulations were performed with a fixed 3-degree blade pitch angle and constant 72 rpm rotational speed. The inlet velocity was equal to 7 m/s, 10 m/s, 15 m/s, and 20 m/s. The angle of attack of the airfoil was varied from 0 to 20 degrees to obtain the lift and drag coefficients curves. The closure turbulence models Unsteady Reynolds-Averaged Navier-Stokes (URANS) were used in both cases. All of the implementations and simulations were developed using the in-house software MFSIM (Multiphysics Simulator). The cartesian-structured block mesh was used to model the fluid dynamics, and the immersed boundary methodology was necessary to model the aerodynamics bodies. Furthermore, using an adaptive grid is a powerful way to save mesh refinement and, therefore, save processing time. Finally, the aerodynamic results showed a good accord with the reference's data, being the measurements made in the NASA AMES wind tunnel for the wind turbine. Therefore, the immersed boundary methodology and adaptative mesh refinement employed in this work proved to be promising computational tools to simulate complex and moving bodies.

Keywords: Immersed Boundary, Aerodynamics, Adaptative Mesh Refinement.

1 Introduction

Due to the worldwide population increase, technological development, and improved standard of living, mainly in industrialized countries, energy consumption has increased by more than ten times since 1900. Thus, society becomes increasingly dependent on this good, which results in the necessity of more investments, studies, and research looking for sustainable strategies Geller [1].

In this scenario, over the past few years, there has been high growth in the use of renewable energy sources that have a low environmental impact and high availability for use. Therefore, an energy source that fits this proposition is wind energy.

The Computational Fluid Dynamics (CFD) technique has been constantly evolved over the last few years due to the improvement of numerical methods and the increase in storage and memory of computational tools. Nowadays, it possible to numerically reproduce increasingly complex fluid dynamics simulations. From this perspective, the aerodynamic study of wind profiles using CFD is an essential line of research to understand this object's fluid dynamics, increase its performance, and choose wind rotor profiles with a more efficient design.

Therefore, the objective of this work is analyze the aerodynamics parameters drag and lift coefficient, mechanical torque and fluid dynamics of the NREL $S809$ airfoil and NREL Phase VI wind turbine. The dynamic refinement mesh will be used, where a higher resolution is applied in places where the information gradients are great. The immersed boundary methodology will be used for the communication between the fluid and the

aerodynamic body. The turbulence closure models used were the standard $k-\varepsilon$ models activating the two-layer formulation and the Spalart-Allmaras model.

2 METHODOLOGY

In this section, it will be presented the modelling for mass, linear momentum, and thermal energy balances. The modelling for the immersed boundary method and the closure of turbulence are also presented.

2.1 Mass and linear momentum balances

The mass balance model for incompressible flows is given by Equation (1):

$$\frac{\partial u_i}{\partial x_i} = 0, \tag{1}$$

where u if the velocity component in the i_{th} coordinate direction.
The mathematical model for the linear momentum balance for incompressible flows of Newtonian fluids is given by Equation (2):

$$\rho\frac{\partial u_i}{\partial t} + \rho u_j\frac{\partial u_i}{\partial x_j} = -\frac{\partial p}{\partial x_i} + \frac{\partial}{\partial x_j}\left[\mu\left(\frac{\partial u_i}{\partial x_j} + \frac{\partial u_j}{\partial x_i}\right)\right] + f_i. \tag{2}$$

where $p\ [N/m^2]$ is the pressure, $\rho\ [kg/m^3]$ is the fluid specific mass, $u_i\ [m/s]$ is the i component of velocity vector, $\mu\ [N\cdot s/m^2]$ is the dynamic viscosity, and $f_i\ [N/m^3]$ is the i component of the Eulerian dynamic force vector representing the immersed boundary.

2.2 The immersed boundary formulation

A Lagrangian mesh is used to represent the immersed boundary, which models a body immersed within the fluid flow. One of the main advantages of the immersed boundary method is that it is possible to represent a complex and mobile body inside the flow even when a cartesian mesh is used. In the present work, the multi direct forcing (MDF) method, based on the work of Wang et al. (2008) Wang et al. [2], was used.

A Eulerian forcing field, $f_i\,(x,t)$, is used to modeling the influence of solid boundary over any neighboring fluid particle placed at the position $\vec{x}$. The linear momentum balance for the fluid particle $\vec{x}$ is given by Equation (2), that can be rewritten as follows:

$$\frac{\partial u_i\,(\vec{x},t)}{\partial t} = RHS_i\,(\vec{x},t) + \frac{1}{\rho}f_i\,(\vec{x},t)\,. \tag{3}$$

To model the forcing term $f_i\,(x,t)$, the transient term of Equation (3) is discretized using a first-order Euler method. Although the velocity $\widetilde{u}_i^{n+1}\,(\vec{x},t)$ for a fluid particle is not given, the velocity of the solid interface is generally known. A force is calculated in the Lagrangian point by Eq. (4):

$$F_i^{n+1}\,(\vec{x}_k,t) = \rho\frac{\widetilde{U}_i^{n+1}\,(\vec{x}_k,t) - U_i^*\,(\vec{x}_k,t)}{\Delta t} \tag{4}$$

where $F_i^{n+1}\,(\vec{x}_k,t)$ is the Lagrangian force that the surface exerts over the particle $\vec{x}_k$, forcing these particles to have the same velocity $\widetilde{U}_i^{n+1}\,(\vec{x}_k,t)$ of the solid surface. The Lagrangian velocity $U_i^*\,(\vec{x}_k,t)$ of a particle placed close to the solid surface is obtained by the interpolation of the Eulerian velocity estimation $u_i^*\,(\vec{x},t)$ as given by Equation (5):

$$U_i^*\,(\vec{x}_k,t) = \sum_{\Omega} u_i^*\,(\vec{x},t)\,D_h\,(\vec{x}-\vec{x}_k)\,h^3. \tag{5}$$

In Equation (5), the summation must be performed over the Eulerian domain, Ω, using a compact support Dirac Kernel, $D_h\,(\vec{x}-\vec{x}_k)$. Equation (4) provides a measure of the velocity difference between a fluid particle that is placed at the surface and the velocity of the surface itself. This difference is converted into a Lagrangian force. The Lagrangian force calculated using Equation (4) can be distributed from the Lagrangian domain Γ to the Eulerian domain Ω:

$$f_i^{n+1}(\vec{x},t) = \sum_{\Gamma} F_i^{n+1}(\vec{x}_k,t)\, D_h(\vec{x}-\vec{x}_k)\, h^3. \tag{6}$$

More details of the immersed boundary method is presented in [3]

2.3 Closure turbulence models

To model the turbulence closure problem we use two models: Spalart-Allmaras model and the Standard k-ε. The turbulence closure model proposed by Spalart and Allmaras Spalart and Allmaras [4] is a one-equation model with which it is possible to solve a modelled balance equation for the kinematic eddy turbulent viscosity. The Spalart-Allmaras model was designed specifically for aerospace applications involving wall-bounded flows and has been shown good results for boundary layers subjected to adverse pressure gradients. It is also gaining popularity in turbo-machinery applications.

The standard $k-\varepsilon$ model, proposed by Launder and Spalding [5] is another URANS turbulence closure model used in the present work. Historically, good results were obtained using the standard $k-\varepsilon$ model in computational simulations of free shear flows and high Reynolds number flows with small adverse pressure gradients. When is desired to simulate wall flows using the standard $k-\varepsilon$ model, an additional model is required for near-wall regions. In the present work, the two-layer wall treatment was used.

3 Results and Discussion

3.1 Wind Rotor Profile

In the Figure 1, it can be seen the immersed boundary, the computational domain, and the mesh in the initial condition. The computational domain has $32m$ in the x-axis, $16m$ in the y-axis, and $1m$ in the z-axis. The mesh in the coarse level has $128 \times 64 \times 4$ volumes. The eulerian mesh has seven physical levels of refinement, and the refinement made in the immersed boundary has the same seven levels of refinement. The airfoil has one meter of chord and is fixed in $x = 8m$, $y = 8m$ and $z = 0m$. At the inlet, Dirichlet condition was used and at the outlet, the advective condition was considered. In the span-wise direction, periodic boundary condition was used and at the bottom and top walls the Neumann condition was applied.

The computational experiments were performed with fix Reynolds number $Re = 1.10^6$ and the angle of attack was varied from $0°$ until $20°$. The drag coefficients and lift coefficients results are depicted in Figure 2-a and Figure 2-b, respectively. The results are compared with experiments made in a wind tunnel in the Ohio State University (OSU) and Deft University Technology (DUT).

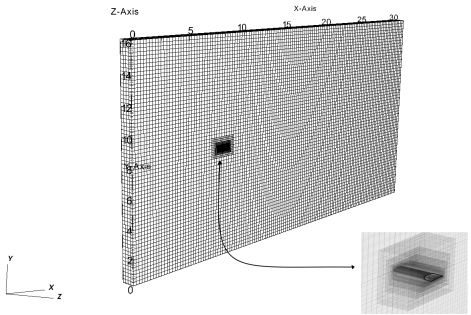

Figure 1. Computational Domain and Mesh Refinament - Initial Condition

Analyzing the Figure 2-a it is noted that until $\alpha < 12°$ the drag coefficient C_d to both turbulence closure models are close to the results obtained in the material experiment. As the angle of attack increased, the same happens to C_d for both curves of computational experiments, In OSU a greater increase in drag was observed from $\alpha \cong 17.5°$ on the other hand, the DUT curve had already been stabilized for this value of α. The results for both turbulence closure models were close to each other, and in $\alpha = 20°$, these curves provided results very close to the curve by OSU.

Examining Figure 2-b, it is observed that the values of lift coefficient for the turbulence closure models reproduced in the present study provided bottom results to the material experiment, although the curves have the

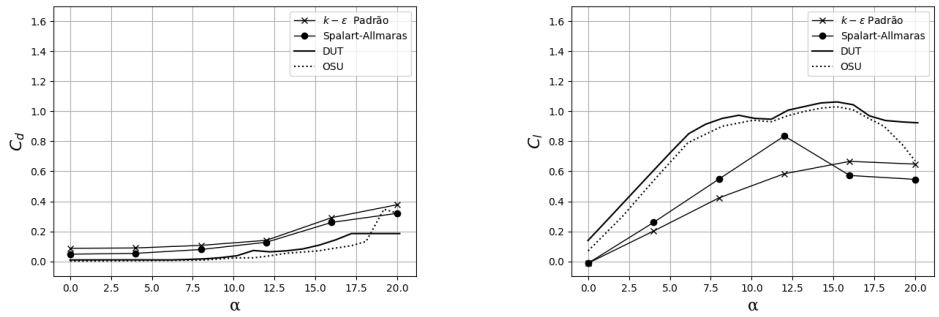

(a) Standard $k - \varepsilon$ (b) Spalart-Allmaras

Figure 2. Drag and Lift Coefficient - $s809$ airfoil

same tendency, especially for the curve obtained for OSU. For low angles of attack $\alpha \leq 12°$, the lift coefficient increases as the angle of attack increases, in an almost linear relationship, because the flow remains attached over the entire airfoil surface, and at $\alpha > 12°$, the C_l for both turbulence closure models started to decrease or stagnate due to the occurrence of boundary layer separation. The model Spalart-Allmaras gives the best results up to $\alpha = 12°$, when the results are decreasing. For the $k - \varepsilon$ model, at the beginning of boundary layer separation until massive flow separation, there is a slight decrease in C_l at $\alpha = 20°$.

The velocity fields for $\alpha = 0°$ and $\alpha = 20°$ for the turbulence closure models standard $k - \varepsilon$ and *Splart-Allmaras* are depicted in the Figure 3 and Figure 4, respectively. Also are presented the mesh who dynamically adapts to the flow for both cases.

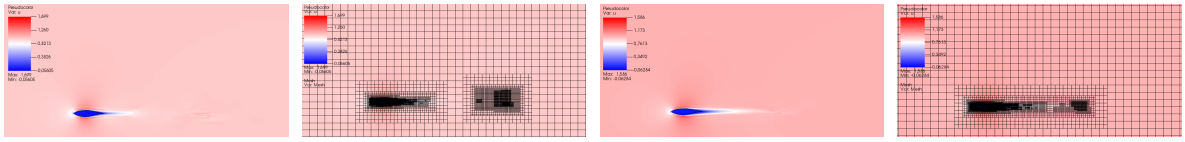

(a) *Spalart-Allmaras*, Velocity Field (b) *Spalart-Allmaras*, Adaptive Mesh (c) Standard, Velocity Field (d) Standard $k - \varepsilon$, Adaptive Mesh

Figure 3. Velocity Field and Mesh Refinement - $\alpha = 0°$

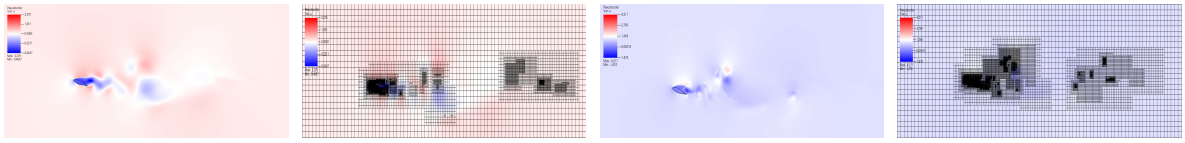

(a) *Spalart-Allmaras*, Velocity field (b) *Spalart-Allmaras*, Adaptive Mesh (c) Standard $k - \varepsilon$, Velocity field (d) Standard $k - \varepsilon$, Adaptive Mesh

Figure 4. Velocity Field and Mesh Refinement - $\alpha = 20°$

Viewing the set of pictures of Fig. 3 and the graphics of the Fig. 2-a and Fig. 2-b, it is clear that for the angle of attack $\alpha = 0°$ the flow develop attached in the surface of the airfoil, where there is not the presence of the separation zones, and, for both turbulence closure models the value for C_l is close to 0 because the low value for the maximum camber, which is just $1°$, therefore the $s809$ model does not have so much asymmetry between the suction side and presssure side of the airfoil. The fluid dynamics change dramatically when $\alpha = 20°$ in the Fig. 4, in this case the separation zone moves toward the leading edge, and there is not the reattachment of the flow, therefore, the flow shedding entirely over the surface and the stall occurs. This phenomenon could be seen graphically by the Fig. 2-a and Fig. 2-b, when the C_d has a great increase and the C_l decrease.

Regarding to the computational technique employed for the adaptative refinament dynamic, it is observed that a larger resolution of a mesh is applied correcty over the regions of interest, in which are close to the immersed boundary and in the wake zones, where there is the presence of turbulent structures. It is also inferred the great savings in memory and processing time, when comparing the region where the refinement occurs in relation to the total computational domain, which is mostly covered by the mesh at the coarsest level.

3.2 Wind Turbine

The computational simulations involving the wind turbine was performed with free stream velocity $U = 7m/s, 10m/s, 15m/s$ e $20m/s$ to each turbulence closure models. The cross-secional area has approximately the same dimension of the wind tunnel NASA/AMES $x = 24m \times z = 36m$ and $80m$ to the domain in the perpendicular direction of the wind turbine. The mesh in the coarsest level has $48 \times 64 \times 160$ volumes. The immersed boundary is positioned in $x = 0m$, $y = 20m$ e $z = 18m$. The height of the tower is $12,2m$ and $10,058m$ of the diameter of the rotor, the blade pitch angle is $\beta = 3°$. Were defined five physical levels to the adaptative mesh, where the finest level follow the movement of the rotor, the turbulent structures in the wake zone are composed of two levels upon the level defined to the immersed boundary. The computational domain and the immersed boundary in the initial condition are illustrated in Fig. 5 and the graphical curves to the mechanical torque are illustrated in Fig. 6 together with the wind tunnel experiment results and the computational simulations made by Benjanirat and Sankar [6] which obtained for the results for the same turbulence models used in the present study.

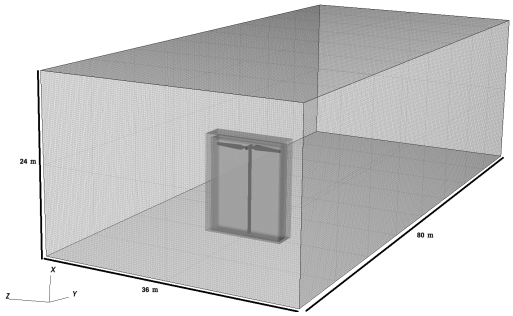

Figure 5. Computional Domain and Immersed Boundary

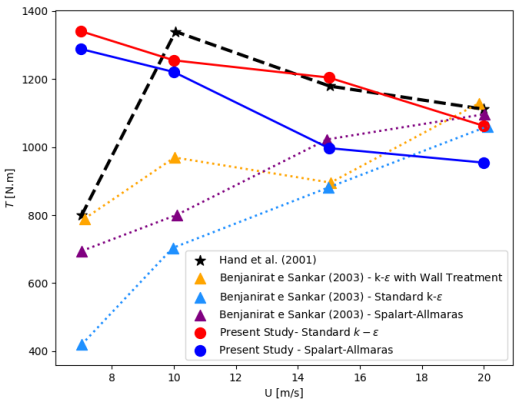

Figure 6. Mechanical Torque

Viewing the graphical results of Fig. 6, in a general manner, the $k - \varepsilon$ closure turbulence models provided the best results compared with the Spalart-Allmaras. Also, It is possible to notice that from $U = 10m/s$ both turbulence closure models have the same trend from the material experiment. Although, both models fail to predict the mechanical torque from $U = 7m/s$. One of the reasons of this high value can be associated with the qualitative differences observed in the present simulations with the experiment made in wind tunnel.

In $U = 7m/s$, as it was observed in the airfoil case, both turbulence models presented a premature boundary layer separation, while in the wind tunnel the flow remains attached over the entire surface of a blade, therefore, when the free stream velocity increase from $U = 7m/s$ to $U = 10m/s$, the increase of the torque happens, although, when the free stream velocity changes to $U = 10m/s$ until $U = 20m/s$, the torque gradually decrease due the increase of separation zones observed over the surface blade, and hence the stall occurs. When the separation is intensified, the drag forces increase, and according to Benjanirat and Sankar [6], the power and torque are highly influenced by this force.Therefore, for this operation range, the methodology employed in this present work could not be enough to capture the physical phenomena in the low Reynolds number, presenting behavior that was expected to happen with larger free stream velocity. Thus, the torque for both turbulence closure models showed a decreasing trend with the increase of the velocity, which is compatible with wind tunnel measurements only from $U = 10m/s$.

Seeing the results only provided by the Benjanirat and Sankar [6], It is evident that the $k-\varepsilon$ with wall treatment generated the results closely to the wind tunnel results, similarly with the present study. In $U = 10m/s$ and $U = 15m/s$ the $k-\varepsilon$ and Spalart-Allmaras from the present study gave the best results, especially in $U = 15m/s$, in which the $k-\varepsilon$ has a difference only $2,13\%$ from the results provided by wind tunnel. On other hand, in $U = 20m/s$ all the curves obtained in Benjanirat and Sankar [6] gave the best predictions, but the value obtained in Standard $k-\varepsilon$ from the present study is quite close.

In the Fig. 7 and Fig. 8 are depicted the iso-value for vorticity in y-direction for the turbulence closure models Standard $k-\varepsilon$ and Spalart-Allmaras, respectively.

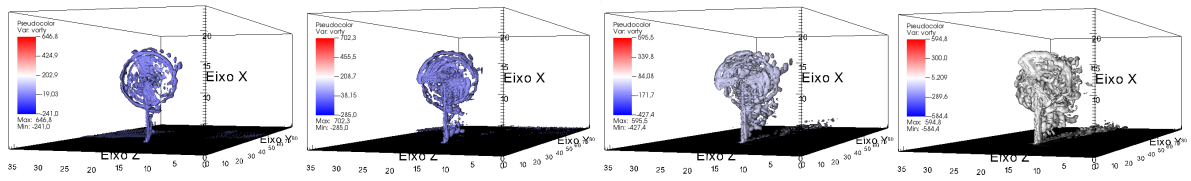

(a) $U = 7m/s$ (b) $U = 10m/s$ (c) $U = 15m/s$ (d) $U = 20m/s$

Figure 7. Vorticity in y-direction - $k-\varepsilon$ Padrão

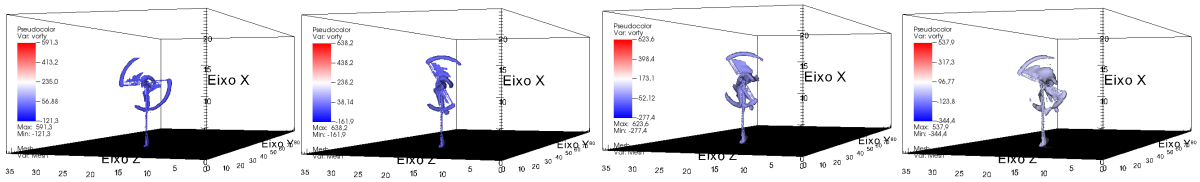

(a) $U = 7m/s$ (b) $U = 10m/s$ (c) $U = 15m/s$ (d) $U = 20m/s$

Figure 8. Vorticity in y-direction - Spalart-Allmaras

Analyzing the set of images in Fig. 7 and Fig. 8, it is perceived, in a general manner, a clear difference in the configuration of the turbulent structures between the closure models used. Although, for both models, it is possible to see that the primary turbulent structures are formed near the immersed boundary, and, is already seen premature separation zones in the surface of the blade for $U = 7m/s$, especially for the Standard $k-\varepsilon$.

In Fig. 7-a a larger turbulent structure in the tip of the blade is notice, in which is transported by the flow, forming structures of helicoidal format. This structure is formed because the influence of centrifugal acceleration in which the flow moves from the root towards the tip of the blade. As the velocity U increase, this pattern are less perceptible for $k-\varepsilon$ model, because with the lower value of turbulent viscosity ν_t compared with the Spalart-Allmaras, therefore, with higher values of kinetic energy and massively flow separation, intensifies the promotion of secondary turbulent structures and interaction non-linear between them in the wake region. For the same reason, in the Spalart-Allmaras is easier to identify this primary rotative structure in the tip of the blade for all the velocity U used. In this model, the turbulent structures are damped because of the dissipative behavior of this model with high turbulent viscosity.

The velocity field in side view together with the mesh refinament in $U = 20m/s$ for both turbulence closure models are illustrated in 9.

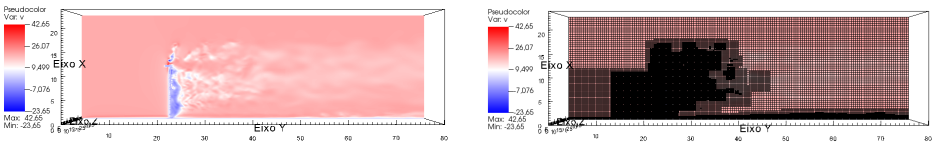

(a) Standard $k-\varepsilon$

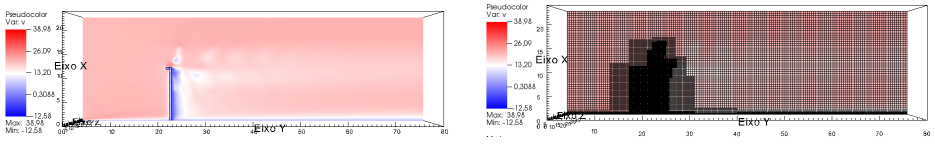

(b) *Spalart-Allmaras*

Figure 9. Side View with the presence of the refinament mesh adaptative - $U = 20m/s$

For the Spalart-Allmaras model, the refinement is applied only near the wind turbine, where only a few meters downstream is identified the presence of turbulent structures, besides, in the ground, where the no-slip condition is defined, there is the creation of refinement block across the domain. In the Standard $k-\varepsilon$ besides the refinement be correctly applied in the ground and near the immersed boundary, It is also applied in the wake zones more distant from the wind turbine, where turbulent structures and gradients are present. As well as the simulations involving the wind rotor profile, it is clear that compared with the maximum level of refinement applied in the entire computational domain, it is clear to observe that the adaptive refinement technique promotes an excellent saving of memory and processing time where it allows if using a coarse mesh in areas where there is no significant amount of momentum.

4 Conclusions

The objective of this work was to numerically reproduce the wind tunnel tests, referring to the technical report [7]. In this work, the immersed boundary technique with the direct multi-forcing method (MDF) was used in URANS class closure models, with application in aerodynamic bodies, being, fixed and mobile, representing the airfoil model $s809$ and the NREL Phase VI wind turbine, respectively. It is worth noting that to date, the application of this technique aimed at aerodynamics is not found in the literature, and therefore, this work has managed to achieve important contributions to the development of this model. Allied to this technique, it was seen that the adaptive refinement of the mesh was correctly applied in the regions of greatest interest and managed to provide great savings in memory and processing time.

In the case involving the airfoil, both curves of the closure models were able to follow the general trend of the computational experiments, especially in OSU. The values of the C_d were close to the results compared for all tested angles of attack and the C_l, the results were smaller, but, both models were able to predict the boundary layer separation, although precociously to material experiments. At $\alpha = 20^{\circ}$, both models the separation zone has advanced the leading edge, and for that angle, the airfoil has already reached the stall

Regarding the wind turbine, the $k-\varepsilon$ model, similarly to the related computational experiment, was the model that provided the best prediction, with very close results in $U = 15\ m/s$ and $20\ m/s$. Although both models failed to predict torque at $U = 7\ m/s$ due mainly to the model's deficiency in predicting low values of the Reynolds number, as in both models, separation zones were identified on the surface of the blade, which for the wind tunnel experiment, at $U = 7\ m/s$ the flow was completely attached over the entire blade surface.

Acknowledgements. The authors gratefully acknowledge financial support from PETROBRAS, Capes, CNPQ and Fapemig. The authors are also grateful to the mechanical engineering graduate program from the Federal University of Uberlândia (UFU).

Authorship statement. The authors hereby confirm that they are the sole liable persons responsible for the authorship of this work, and that all material that has been herein included as part of the present paper is either the property (and authorship) of the authors, or has the permission of the owners to be included here.

References

[1] H. S. Geller. *Revolução Energética: Políticas para um futuro sustentável*. Relume Dumerá, Rio de Janeiro, 2003.

[2] Z. Wang, J. Fan, and K. Luo. Combined multi-direct forcing and immersed boundary method for simulating flows with moving particles. *International Journal of Multiphase Flow*, vol. 34, n. 3, pp. 283 – 302, 2008.

[3] R. R. S. Melo, D. Kinoshita, M. M. Villar, R. Serfaty, and A. Silveira-Neto. Numerical experiment of turbulent transfer of thermal energy using the immersed boundary method and adaptive mesh refinement. *International Journal of Thermal Sciences*, vol. 151, pp. 106281, 2020.

[4] P. R. Spalart and S. R. Allmaras. A one-equation turbulence model for aerodynamic flows. *AIAA Paper*, 1992.

[5] B. E. Launder and D. B. Spalding. *Lectures in Mathematical Models of Turbulence*. Academic Press, 1972.

[6] S. Benjanirat and L. N. Sankar. Evaluation of turbulence models for the prediction of wind turbine aerodynamics. *American Institute of Aeronautics and Astronautics (AIAA) Paper*, 2003.

[7] M. Hand, D. Simms, L. Fingersh, D. Jager, J. Jager, J. Cotrell, S. Schreck, and S. Larwood. *Unsteady Aerodynamics Experiment Phase VI: Wind Tunnel Test Configurations and Available Data Campaigns*. NREL/TP-500-29955. National Renewable Energy Laboratory, Golden, Colorado, 2001.